Structural Characterization of New Nanocomposite Hybrid Materials: Organic Nanocrystals Grown in Gel−Glasses

Nathalie Sanz,[†] Pierre Terech,[‡] David Djurado,[§] Bruno Demé,[||] and Alain Ibanez*,[†]

Laboratoire de Cristallographie, CNRS, UPR 5031, associée à l'Université J. Fourier et à l'INPG, BP 166, 38042 Grenoble Cedex 9, France, Laboratoire Physico-Chimie Moléculaire, UMR 5819 CEA−Grenoble, 17 rue des Martyrs, 38054 Grenoble Cedex 09 France, Laboratoire de Spectrométrie Physique, Université Joseph Fourier, CNRS (UMR 5588), BP 87, 38402 Saint Martin d'Hères Cedex, France, and Institut Laue Langevin, BP 156, 6 rue Jules Horowitz, 38042 Grenoble Cedex 09, France

Received October 28, 2002. In Final Form: January 13, 2003

We have engineered new hybrid organic−inorganic materials through a generic and flexible preparation of stable organic nanocrystals grown in gel−glass matrixes for optics. Host matrixes display a microporous porosity from 0.7 to 1.6 nm depending on silicon alkoxydes and solvents used. Organic nanocrystals have been characterized by different coupled techniques and present average sizes from 10 to 27 nm according to dye molecules and molar concentration. When a magnetic field is applied during the nanocrystallization process, organic crystals exhibit larger average sizes due to a better molecular aggregation.

1. Introduction

Organic crystals exhibit various appropriate properties such as luminescence, photochromism, or high nonlinear optical (NLO) efficiency due to the high polarizability of π-conjugated molecules.[1] In addition, these organic compounds possess unlimited molecular engineering possibilities, which allow the improvement of these optical properties. To take advantage of the optical properties of molecular crystals and to design materials with enhanced stability, we have developed the nanocrystallization of organic phases in inorganic gel−glasses.[2−5] Sol−gel matrixes (bulk or thin films) are known, since 1984,[6] to be favorable to the insertion of organic molecules through sol−gel chemistry methods. Indeed, inorganic matrixes can be prepared at room temperature by using sol−gel reactions compatible with organic media. Until now, molecules were dispersed within or grafted onto sol−gel networks.[6−8] In the present work we show how organic molecules can be aggregated through confined nucleation and growth to form crystals in the pores of the gel matrix. This generic process leads to the preparation of a new type of hybrid organic−inorganic materials made up of organic nanocrystals grown in amorphous inorganic matrixes. These nanocomposite materials combine not only the optical properties of molecular crystals with the stability and transparency of the silicate matrixes but also the advantages of crystals (size effects, noncentrosymmetry) with those of amorphous phases (convenient processing and shaping of bulk samples or thin films). These samples exhibit good transparency due to the homogeneity of the silicate matrix and the nanometer scale of included dye crystals. Their NLO or luminescence properties have been first targeted[2−5,9] while the specimens are rigid solids which can be easily sliced and polished for optical characterizations. It was shown that chemical stability and photostability of nanocrystals are improved with respect to isolated molecules in solutions or matrixes.[9]

The crystalline quality of the organic aggregates has been first demonstrated by well-defined melting peaks observed in differential scanning calorimetry (DSC) while their sizes were determined by transmission electron microscopy (TEM) experiments. Two typical structural behaviors were observed for the bulk nanocomposite materials:[10]

On one hand, when the interactions existing between the dye molecules on the nanocrystal surface and the silicate matrix are weak (van der Waals bonds), as in the case of 4,4′-sulfonyldiphenol (SDPH), the corresponding interfacial structure observed by TEM is sharp and the nanocrystals melt below the bulk melting point of the dye.

And on the other hand, when the dye−matrix interactions are strong, as due by many short H-bonds between the molecules on the nanocrystal surface and the matrix, the interfacial structure is fuzzy as in the case of the *N*-4-nitrophenyl-L-prolinol (NPP) for example. This is in agreement with the ill-defined NPP particles observed by TEM and with a great superheating of these nanocrystals in comparison to the bulk melting point of NPP. Thus, the thermal stability of organic nanocrystals can be greatly

* To whom correspondence may be addressed. Tel: 33 476 88 78 05. Fax: 33 476 10 38. E-mail: alain.ibanez@grenoble.cnrs.fr.

[†] Laboratoire de Cristallographie, CNRS, UPR 5031, associée à l'Université J. Fourier et à l'INPG.

[‡] Laboratoire Physico-Chimie Moléculaire, UMR 5819 CEA−Grenoble.

[§] Laboratoire de Spectrométrie Physique, Université Joseph Fourier, CNRS (UMR 5588).

[||] Institut Laue Langevin.

(1) Chemla, D.; Zyss, J. *Nonlinear Optical Properties of Organic Molecules and Crystals*; Academic Press: Orlando, FL, 1987; Vols. 1 and 2.

(2) Ibanez, A.; et al. *Adv. Mater.* **1998**, *10*, 1540−1543.

(3) Sanz, N.; Baldeck, P. L.; Ibanez, A. *Synth. Met.* **2000**, *115*, 229−243.

(4) Sanz, N.; et al. *J. Mater. Chem.* **2000**, *10*, 2723−2726.

(5) Sanz, N.; et al. *Appl. Phys. Lett.* **2001**, *78* (*17*), 2569−2571.

(6) Avnir, D.; Levy, D.; Reisfeld, R. *J. Phys. Chem.* **1984**, *88*, 5957−62.

(7) Sanchez, C.; Ribot, F. *New J. Chem.* **1994**, *18*, 1007−47.

(8) Avnir, D.; Kaufman, V. R.; Reisfeld, R. *J. Non.-Cryst. Solids* **1985**, *74*, 395−406.

(9) Sanz, N. *Solid State Sci.* **2001**, *3* (8), 867−875.

(10) Sanz, N.; Boudet, A.; Ibanez, A. *J. Nanopart. Res.* **2002**, *4*, 99−105.

10.1021/la020878z CCC: $25.00
Published on Web 03/12/2003

improved by the confined growth of the dye in the pores of a dense sol−gel matrix through dye−matrix interactions. On the other hand, the crystalline quality of the organic particles has been confirmed by fluorescence and second harmonic generation spectroscopies.[2,11]

In this paper, we present structural characterizations carried out for SDPH and NPP nanocrystals which exhibit weak and strong dye−matrix interactions, respectively. We have specified the microporosity of the silicate matrixes by gas adsorption−condensation experiments while X-ray diffraction and small-angle neutron scattering experiments have been used in order to obtain a global characterization of the nanocrystal sizes and nanocrystal−matrix interfacial structures.

2. Preparation of NPP and SDPH Nanocrystals Grown in Sol−Gel Matrices

The preparation of organic nanocrystals grown in the pores of sol−gel matrixes has been described elsewhere.[2−4] The polymeric gels are obtained from silicon alkoxides such as tetramethoxysilane (TMOS) according to the procedure of ref 12. These silicate matrixes exhibit silanol functions (≡SiOH) which can form hydrogen bonds with the organic nanocrystals. If these dye−matrix interactions are too strong, the molecular aggregation and the crystalline structure of the resulting nanocrystals can be significantly disturbed.[4] To reduce these dye−matrix interactions, methyltrimethoxysilane (MTMOS) is added to the TMOS precursor. Indeed, the nonbridging methyl functions, arising from MTMOS, are not hydrolyzed and cover the gel pores to screen the remaining silanol functions of the xerogel matrix.[13,14] Thus, hybrid nanocomposite samples of high optical quality are obtained from the TMOS precursor and 0.4TMOS + 0.6MTMOS molar mixtures. Nevertheless, to avoid the common problems of crack formation, due to capillary strength,[12] the gels are slowly dried at room temperature. To reduce the drying time and to increase the elasticity of the resulting xerogels, we have optimized a new ORMOSIL (ORganically MOdified SILicate) matrix. We added to the previous sol−gel matrixes around 5 molar percents of the silicone polydimethylsiloxane (PDMS). This silicone involves 14 methyl groups per monomer unit. These organic groups lead to a better elasticity of the matrix by holding up constraints in compression due to capillary strengths. In addition, gas adsorption−condensation measurements (see next section) show that the average pore size of the matrix increases with the number of nonbridging methyl groups which point out into the pores of the matrix. This decreases the capillary constraints since the capillary pressure is inversely proportional to the pore diameter.[15]

The initial solutions, constituted by silicon alkoxides, an organic solvent, and a small amount of water, were introduced with the dye powder in airtight cells and heated at 80 °C. Each selected organic solvent (ethanol for SDPH and acetonitrile for NPP) allows both to dissolve each dye molecules and to make miscible the hydrolysis water with the silicon alkoxides. The molar concentration of the solvent is equal to that of silicon alkoxides. Homogeneous sols were obtained at 80 °C within a few minutes and formed gels after several hours. The hydrolysis and condensation reactions were carried out under acidic conditions (HCl) with 1 H_2O molecule per alkoxide ($-OCH_3$) function. The gels were then aged at 80 °C during 48 h to adjust the gel porosity. Then, a supersaturation of the dye in the solvent is applied by lowering the temperature at 20 °C. This supersaturation status induces a sudden nucleation of the organic phase in the pores of the gel which act as nanometer scaled reactors for the crystal growth in solution. This process, based on the La Mer's diagram,[16] leads to narrow size distributions of the nanocrystals.

To obtain monolithic xerogels, the samples were slowly dried at room temperature during 6, 4, and 1 weeks for xerogels obtained from TMOS, 0.4TMOS + 0.6MTMOS, and 0.57TMOS + 0.38MTMOS + 0.05PDMS mixed precursors, respectively. The corresponding hybrid nanocomposite samples are labeled, for example, in the case of SDPH nanocrystals, SDPH/TMOS, SDPH/TMOS + MTMOS, and SDPH/TMOS + MTMOS + PDMS, respectively. Finally, the samples were annealed at temperatures close to the melting point of the organic phase to improve the crystallinity of nanocrystals and to remove residual solvents. The resulting monolithic nanocomposite samples (disks of 12 mm diameter and 3−5 mm thickness) exhibit high optical quality as evidenced by their transparency.

The dye concentrations, which are directly related to the applied supersaturations, were specified by the molar ratio d = [dye]/[silicon alkoxides], d varies from 0.08 to 0.09 for SDPH/TMOS + MTMOS + PDMS and from 0.01 to 0.04 for NPP/TMOS + MTMOS + PDMS and is 0.07 for NPP/TMOS + MTMOS.

3. Gas Adsorption−Condensation: Porosity Measurements

Nitrogen adsorption−desorption isotherms for TMOS, 0.4TMOS + 0.6MTMOS and 0.57TMOS + 0.38MTMOS + 0.05PDMS dried gels prepared in ethanol (Figure 1a) and acetonitrile (Figure 1b) have been measured. According to the original BDDT classification[17] isotherms obtained for the one-step acid-catalyzed xerogels are of type I, characteristic of microporous solids, which present a pore size of less than 2 nm diameters. Surface area and microporous volume are deduced from these adsorption−desorption isotherms by calculating the adsorption and desorption kinetics of nitrogen adsorbed onto the surfaces of the pores by condensation at 77 K. Results are summarized in Table 1. First, for all types of matrixes, the acetonitrile solvent tends to reduce the surface area and the microporous volume of xerogels in comparison to ethanol. The 0.4TMOS + 0.6MTMOS matrixes present a microporous volume larger than that with TMOS xerogel. Indeed, the nonbridging $Si-CH_3$ functions arising from the MTMOS precursor lead to more open microporous structures.[4] On the other hand, the microporous volume of the 0.57TMOS + 0.38MTMOS + 0.05PDMS xerogels prepared in ethanol is 10 times smaller than those obtained from the other gel−glasses (Figure 1a, Table 1). Furthermore, when 0.57TMOS + 0.38MTMOS + 0.05PDMS matrix is prepared in acetonitrile, no evidence of open porosity is observed.

Moreover, the pore size distributions are calculated by differentiation of the pore volume adsorbed with respect to the pore size by using the model of Horvath−Kawazoe.[18,19] This model is suitable for pores having diameters

(11) Treussart, F.; Botzung-Appert, E.; Dong, T. A.; Roch, J. F.; Ibanez, A.; Pansu, R. Submitted to *Chem. Phys. Lett.*

(12) Brinker, C. J.; Scherer, G. W. *Sol−Gel Science, The Physics and Chemistry of Sol−Gel Processing*; Academic Press: Boston, MA, 1990.

(13) Schmidt, H.; Scholze, H.; Kaiser, A. *J. Non-Cryst. Solids* **1984**, *63*, 1−11.

(14) Scholze, H. *J. Non-Cryst. Solids* **1985**, *73*, 669−680.

(15) Scherer, G. W. *J. Non-Cryst. Solids* **1990**, *121*, 104−109.

(16) La Mer, V. K.; Dinegar, R. H. *J. Am. Chem. Soc.* **1950**, *17*, 4847−4854.

(17) Brunauer, S.; Emmett, P. H.; Teller, E. *J. Am. Chem. Soc.* **1938**, *60*, 309.

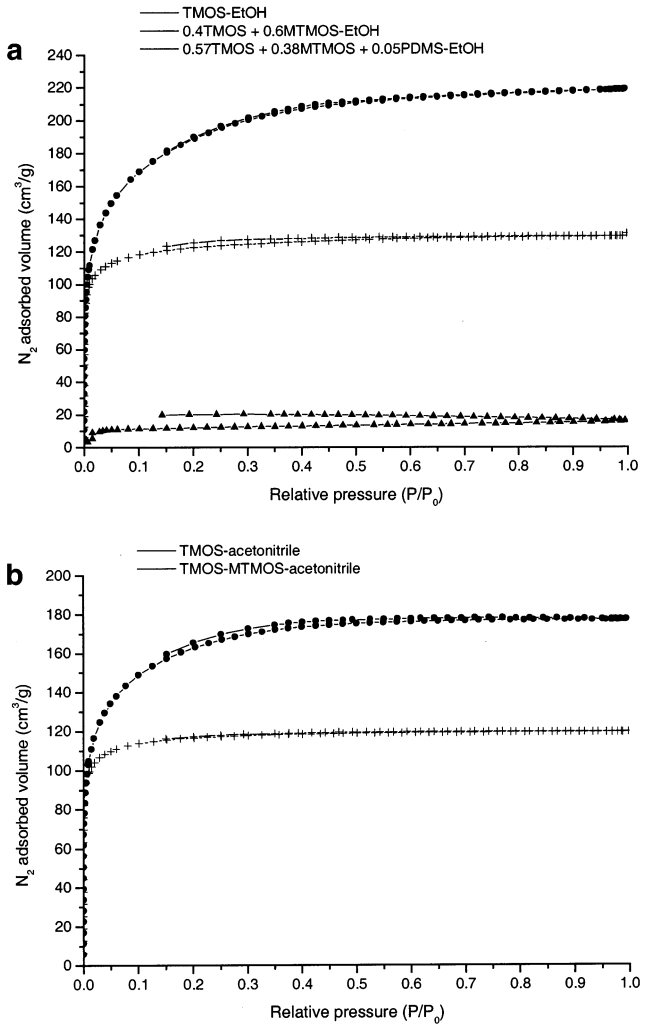

Figure 1. (a) N_2 adsorption and desorption isotherms performed at 77 K for TMOS, 0.4TMOS + 0.6MTMOS, and 0.57TMOS + 0.38MTMOS + 0.05PDMS xerogels prepared in ethanol. (b) N_2 adsorption and desorption isotherms performed at 77 K for TMOS and 0.4TMOS + 0.6MTMOS xerogel prepared in acetonitrile.

Table 1. Specific Area and Microporous Volume of TMOS, 0.4TMOS + 0.6MTMOS, and 0.57TMOS + 0.38MTMOS + 0.05PDMS Xerogels Prepared in Ethanol and TMOS and 0.4 TMOS + 0.6MTMOS Xerogels Made in Acetonitrile

samples	specific area (m^2/g)	microporous vol (cm^3/g)
TMOS (EtOH)	524	0.1950
0.4TMOS + 0.6MTMOS (EtOH)	782	0.3386
0.57TMOS + 0.38MTMOS + 0.05PDMS (EtOH)	53	0.0246
TMOS (acetonitrile)	510	0.1848
0.4TMOS + 0.6MTMOS (acetonitrile)	708	0.2741
0.57TMOS + 0.38MTMOS + 0.05PDMS (acetonitrile)	~0	~0

less than 1.6 nm and thus is only relevant for TMOS and 0.4TMOS + 0.6MTMOS prepared in ethanol (Figure 2a) and in acetonitrile (Figure 2b). The xerogels prepared from the TMOS precursor exhibit a narrower pore size distribution and lower average pore size (0.7 nm) than those obtained with the 0.4TMOS + 0.6MTMOS mixture (1.1 nm), Table 2.

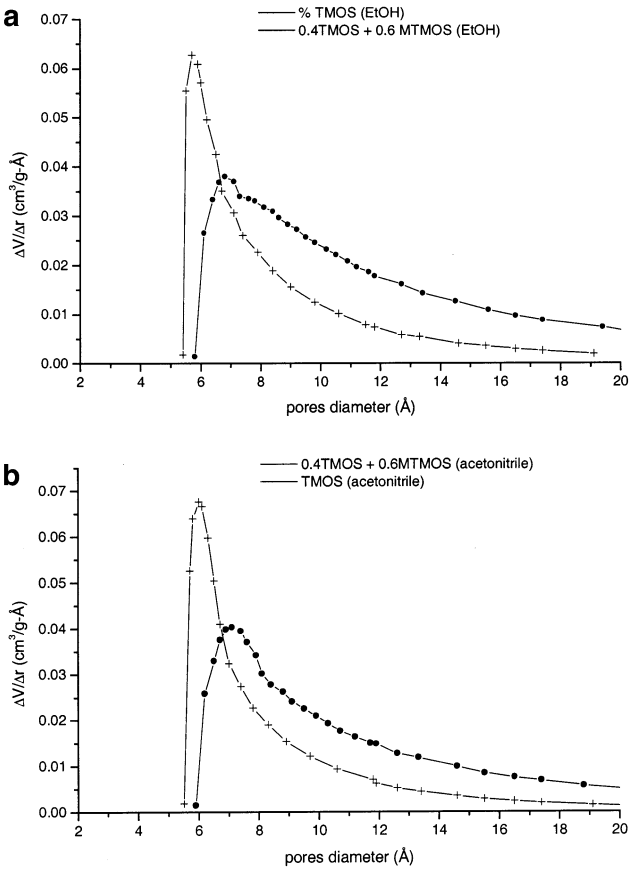

Figure 2. (a) Pore size distributions calculated by the Horvath−Kawazoe model for TMOS and 0.4TMOS + 0.6MTMOS xerogels in ethanol. (b) Pore size distributions calculated by the Horvath−Kawazoe model for TMOS and 0.4TMOS + 0.6MTMOS xerogels in acetonitrile.

On the other hand, the DFT quantum chemistry method (density functional theory)[20−22] allowed, from the experimental adsorption−desorption isotherms, the accurate confirmation of these pore size results for TMOS and 0.4TMOS + 0.6MTMOS samples (Table 2) but also the characterization of the larger pores (diameters more than 1.6 nm) of the 0.57TMOS + 0.38MTMOS + 0.05PDMS xerogel prepared in ethanol (Figure 3a). The DFT calculations (DFT plus software, Micromeritice, version 2.02) are made by comparing our adsorption−desorption isotherms to those of reference materials which are rather close to our sol−gel matrixes (DFT plus models 2.02) like MCM41, which is a porous silica where pores exhibit a cylindrical geometry. Similar porosities are obtained for ethanol and acetonitrile preparations and two maxima can be observed on the pore size distributions curve (Figure 3): the first peak is centered around 0.6−0.7 nm and the second one is at 1.2−1.3 nm, Table 2. The pore size distribution of TMOS xerogel, which varies from 0.5 to 3 nm, exhibits a sharper curve, while the 0.4TMOS + 0.6MTMOS distribution is extended from 0.5 to 4 nm in agreement with the first results obtained with the Horvath−Kawazoe model (Figure 2). This confirms the more open structure of the 0.4TMOS + 0.6MTMOS matrix compared to that of TMOS due to the nonbridging methyl groups. In all cases, the pore diameters are less than 4

(18) Saito, A.; Foley, H. C. *AlChE J.* **1991**, *37*, 429.
(19) Horvath, G.; Kawazoe, K. *J. Chem. Eng. Jpn.* **1983**, *16*, 470.
(20) Olivier, J. P.; Conklin, W. B. In *Internatianol Symposium on the Effects of Surface Heterogeneity in Adsorption and Catalysis on Solids*, 1992. Poland.
(21) Olivier, J. P. *J. Porous Mater.* **1995**, *2*, 9.
(22) Balbuena, P. B.; Gubbins, K. E. *Fluid Phase Equilibra*; Elsevier: Amsterdam, 1992; Vol. 76.

Table 2. Pore Size Distribution for TMOS, 0.4TMOS + 0.6MTMOS, and 0.57TMOS + 0.38MTMOS + 0.05PDMS Xerogels in Ethanol and Acetonitrile

samples	Horavth−Kawazoe av diameter (Å)/max diameter	EFT diameter at max peak (Å)	distribution
TMOS (EtOH)	7/6	6 and 12	from 4 to 30 Å
0.4TMOS + 0.6MTMOS (EtOH)	11/7	7 and 13	from 5 to 40 Å
0.57TMOS + 0.38MTMOS + 0.05PDMS (EtOH)	nonconvenient	15	from 13 to 19 Å
TMOS (acetonitrile)	7/6	6, 8, and 12	from 5 to 20 Å
0.4TMOS + 0.6MTMOS (acetonitrile)	10/7	7 and 12	from 5 to 35 Å

nm. The 0.57TMOS + 0.38MTMOS + 0.05PDMS xerogel prepared with ethanol presents a single population of pores, centered around 1.5 nm (Figure 3a). Its open microporosity is less important than that of the previous ones, while the 0.57TMOS + 0.38MTMOS + 0.05PDMS xerogel prepared in acetonitrile does not exhibit any open porosity (Table 2).

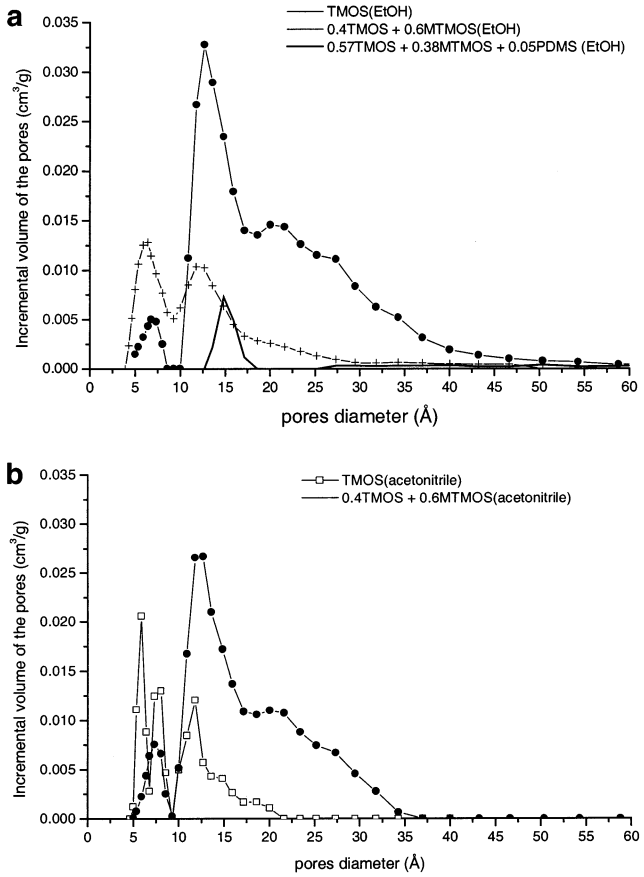

Figure 3. (a) Pore size distributions calculated by DFT method for TMOS, 0.4TMOS + 0.6MTMOS, and 0.57TMOS + 0.38MTMOS + 0.05PDMS xerogels in ethanol. (b) Pore size distributions calculated by the DFT method for TMOS and 0.4TMOS + 0.6MTMOS xerogels in acetonitrile.

4. Wide-Angle X-ray Scattering

Due to the strong absorption of monolithic samples, X-ray measurements have been only performed in a $\theta-2\theta$ reflection geometry (Bragg−Brentano geometry) using a copper anode ($\lambda = 1.5406$ Å). We used a linear detector constituted by 800 channels ($2\theta = 0.02°$ by channel) and the minimal angle of detection is $2\theta = 2°$. X-ray diffractograms were registered by counting 30 s per step. In all cases no diffraction peak could be detected as illustrated by the Figure 4 exhibiting the X-ray diffractogram obtained for NPP nanocrystals grown in the 0.57TMOS + 0.38MTMOS + 0.05PDMS matrix. This is due to the weak scattering factors of the organic phases involved at low concentrations in comparison to the silicate matrixes. Moreover, the small size of the nanocrystals induces a broadening of their corresponding diffraction peaks which does not appear above the X-ray scattering of the inorganic matrix. Thus, diffraction profiles only exhibit typical broad scattering peaks mainly due to the amorphous silicate matrix. Figure 4 shows a large scattering peak centered at 15 nm^{-1}. This corresponds, in real space, to the first average interatomic lengths of about 0.42 nm. This scattering peak is typically observed for the class of silicate xerogels used in this study.[23] For smaller Q values, we observe a scattering peak which corresponds, in real space, to a length of 1.1 nm. This value is nearby the average size of pore diameter found by gas adsorption−condensation. This is likely due to the scattering of the micropores centered around 1.5 nm.

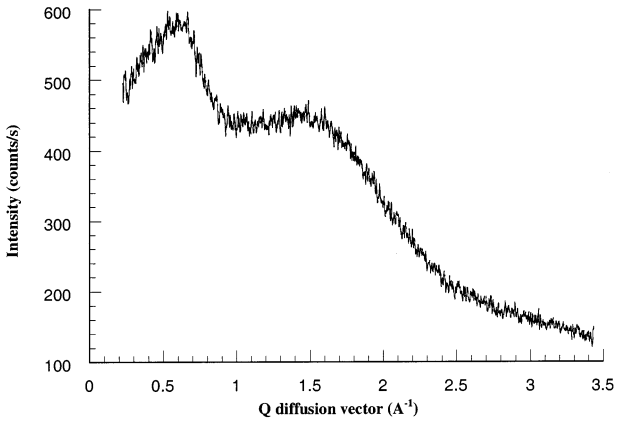

Figure 4. X-ray diffractogram of NPP nanocrystals embedded in a 0.57TMOS + 0.38MTMOS + 0.05PDMS matrix.

5. Small-Angle Neutron Scattering (SANS)

Since the wide- and small-angle X-ray scattering techniques are not well suited due to the weak scattering power of organic molecules compared to that of the silicate matrix, we performed additional SANS experiments at the D11 beam line of the ILL neutron facility in Grenoble, France (all information can be found on http://www.ill.fr). We have used three distances (20, 5, and 1.1 m) at $\lambda = 6$ Å to cover the 0.002−0.3 $Å^{-1}$ range for different xerogels (TMOS, 0.4TMOS + 0.6MTMOS, and 0.57TMOS + 0.38MTMOS + 0.05PDMS) and several types of organic nanocrystals sulfonyldiphenol (labeled SDPH) and *N*-(4-nitrophenyl)-L-prolinol (labeled NPP) grown within these xerogel matrixes.

Figure 5 shows the scattering curves for xerogels with and without nanocrystals. The signal of the silica matrice (without nanocrystals, curve 1) exhibits a sharp low-angle decay (slope between −3.6 and −4) up to 0.004 $Å^{-1}$ followed by a smoother decay (slope ca. −0.55). Nanocomposite samples containing the organic nanocrystals exhibit different scattering profiles (see Figure 5 scattering curves 2, 3, 4, and 5) demonstrating that SANS is appropriate to investigate the nanocrystallization in such inorganic

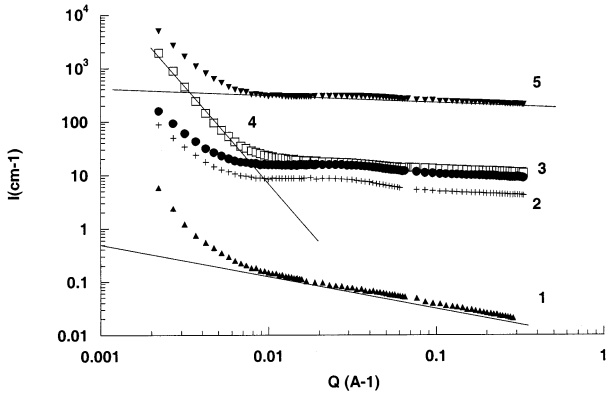

Figure 5. (1) TMOS + MTMOS + PDMS matrix annealed at 80 °C. (2) Idem 1 + SDPH $C = 9\%$. (3) Idem 1 + SDPH $C = 8\%$. (4) Idem 2 but not annealed. (5) Idem 3 but annealed at 240 °C. Indicative slopes are shown (see text).

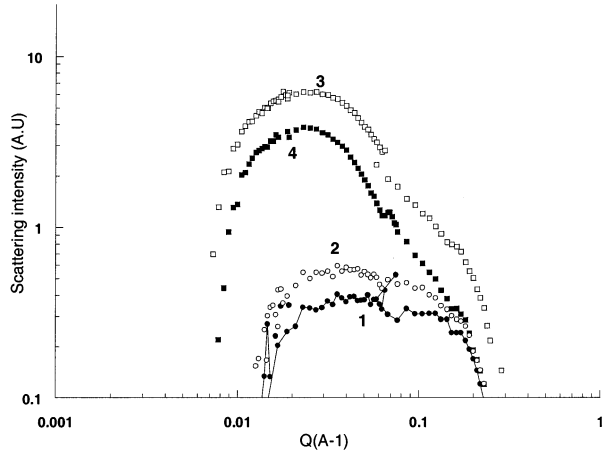

Figure 6. (1) NPP/TMOS + MTMOS + PDMS matrix $C = 1\%$. (2) Idem 1, $C = 4\%$. (3) SDPH/TMOS + MTMOS + PDMS matrix $C = 8\%$. (4) Idem 3, $C = 9\%$.

matrixes. Another remarkable feature in Figure 5 is the existence of a broad bump located at $Q \sim 0.025$ Å^{-1} depending on the treatment of the system (annealing temperature of the xerogel, type of matrix, type of dye molecule, concentration). The average level of scattered intensity is increased by ca. 2000 (for SDPH in a TMOS/MTMOS/PDMS matrix annealed at 240 °C and $d = 0.08$). The slope of the intensity decay of loaded matrixes is decreased from -4 to -0.025 (see Figure 5).

A major difficulty lies in the inability of extracting the signal of the matrix associated to a given organic–inorganic glass since the composite matrix is obtained by simultaneous inorganic polycondensation/organic nanocrystallization reactions. It is most probable that the porous silica structure, which is grown, is affected by the nanocrystal presence. To overcome this inherent limitation, we subtracted first the low-angle part assumed to be representative of the matrix ($I \propto kQ^{-4}$) and using an appropriate numerical procedure. The huge increase in intensity and associated lowering of the dI/dQ slope is attributed to the high level of incoherent scattering due to the protons of the organic molecules ($d \sim 0.04-0.08$) as referred to the gel matrix which contains also a lot of methyl groups. The procedure provides a correlation peak (Figure 6) whose position of the apex corresponds to distances ranging from 10 to 27 nm depending on the dye molecule and concentration used. The curves 1 and 2

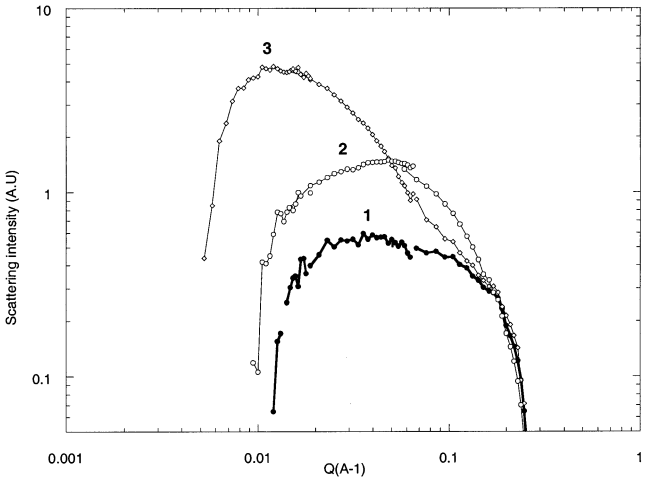

Figure 7. (1) NPP/TMOS + MTMOS + PDMS matrix $C = 4\%$. (2) NPP/TMOS + MTMOS matrix annealed at 80 °C, $C = 7\%$. (3) NPP/TMOS + MTMOS + PDMS matrix $C = 4\%$ magnetic field.

correspond to the scattering of the 0.57TMOS + 0.38MTMOS + 0.05PDMS xerogel with NPP nanocrystals grown within while curves 3 and 4 refer to a similar xerogel with embedded SDPH nanocrystals. Basically, SDPH/TMOS + MTMOS + PDMS samples exhibit a higher scattering level than NPP/TMOS + MTMOS + PDMS likely due to the high SDPH concentration (twice higher than that of NPP). The peak apex for NPP nanocrystals appears around $Q \sim 0.04-0.05$ Å^{-1} while it is at a lower Q value for SDPH nanocrystals, centered around $Q \sim 0.02-0.025$ Å^{-1}. The maximum curve is slightly shifted depending on the concentration for each dye, respectively.

Figure 7 presents the scattering curves of several xerogels with NPP nanocrystals grown within. The same procedure as described previously provides a correlation peak whose position of the apex arises around $Q \sim 0.014-0.045$ Å^{-1}, corresponding to distances ranging from 12 to 48 nm.

At this stage, we focused on the effect of the matrix by carrying on experiments with a TMOS + MTMOS or a TMOS + MTMOS + PDMS xerogel and also on the influence of an external magnetic field during the NPP nanocrystallization. Indeed, these materials, consisting of randomly oriented nanocrystals in amorphous matrixes, are isotropic and centrosymmetric at the wavelength scale ($\lambda \approx 0.4-2$ μm). To break this centrosymmetry and to obtain nanocomposite materials active in second harmonic generation (SHG), we attempted to orient the nanocrystals under a magnetic field.[24] Since many molecules engineered for quadratic nonlinear optics exhibit high dipolar moments, the orientation of nanocrystals can be considered under an electric field. But a high electric field cannot be applied during the nanocrystallization process due to the gel conductivity. For this reason we have applied in a previous study a high magnetic field during the nanocrystallization process. Indeed, due to the diamagnetic susceptibility of the dye molecules[25–27] previous works have demonstrated that organic crystals can be oriented in solution by a magnetic field. After gelation, when the

(23) Himmel, B.; Gerber, Th. *J. Non-Cryst. Solids* **1987**, *91*, 122.

(24) Sanz, N.; Wang, I.; Zaccaro, J.; Beaugnon, E.; Baldeck, P. L.; Ibanez, A. *Adv. Funct. Mater.* **2002**, *12* (5), 352–358.

(25) Astier, J. P.; Veesler, S.; Boistelle, R. *Acta Crystallogr. D* **1998**, *54*, 703.

(26) Ataka, M.; Katoh, E.; Wakayama, N. I. *J. Cryst. Growth* **1997**, *173*, 592.

(27) Krishnan, K. S.; Guha, B.; Banerjee, B. C. *Philos. Trans. R. Soc. London, Ser. A* **1933**, *231*, 235.

temperature is lowered from 80 °C to room temperature (see section 2), the samples were placed in a superconductive coil. At this stage, the pore diameters of the wet gel are significantly higher than those of the final gel glass, lying between 10 and 100 nm.[28] Thus, the nucleation of NPP occurs under a high magnetic field (16 T) and the resulting nuclei are oriented through their diamagnetic anisotropy.

Scattering curves (Figure 7 curves 1 and 3) show clearly a significant shift in the peak position to lower Q values when the magnetic field is applied. This corresponds to a larger average size of 48 nm for NPP nanocrystals prepared under magnetic field to be compared to an average size of 12 nm when no field is applied. Comparison between average sizes of nanocrystals (curves 1 and 3) is made with a similar host−matrix (TMOS + MTMOS + PDMS) and a similar dye concentration ($C = 4\%$). Curve 2 only shows the effect of the matrix (no PDMS added) and the dye concentration ($C = 7\%$).

6. Discussion and Conclusions

First, it has been shown by the present study that the size of the pores in these organically modified xerogels is in the nanometer scale. This has been confirmed by modeling the adsorption−desorption N_2 curves using two different calculations. These pore size values are in good agreement with previous studies carried out on acid-catalyzed xerogels, whatever the solvent involved in the preparation.[12]

Second, wide-angle X-ray scattering curves show a peak centered at $Q = 6$ nm^{-1}. The related length scale corresponds satisfactorily to the microporous porosity scale of the silicate matrix. A second peak appears at a classical Q value of 15 nm^{-1} and is related to the amorphous matrix. No diffraction peaks of organic nanocrystals have been evidenced by WAXS, whereas previous studies[24,29] and in particular calorimetry experiments[10] allowed the observation of melting endothermal peaks of nanocrystals thus proving their crystallinity in the amorphous matrix. Organic nanocrystals cannot be characterized by X-ray diffraction due to their weak scattering factors (low electron density) in comparison to those of the amorphous inorganic matrixes. In addition, the organic nanocrystals are involved at low relative molar concentrations in the silicate matrixes (d = organic/alkoxide $\approx 10^{-2}-10^{-1}$). Thus, sizes of the organic nanocrystals have been measured by coupled studies involving TEM and SANS.

SANS experiments suggested that NPP nanocrystals have average size of 10−13 nm while SDPH nanocrystals present a larger size around 25−27 nm. These measurements are in good agreement with TEM observations.[10] We observed that TEM experiments have provided micrographs showing nanocrystals with a size distribution of 10−30 nm. Furthermore useful information was also extracted from DSC and NMR techniques to estimate the particle−matrix interactions and the crystallinity of the organic aggregates.[27] In this previous study we have shown that NPP nanocrystals present hydrogen bonds via the nitro group with the residual silanol functions of the host matrix while SDPH exhibits weakest van der Waals interactions with the matrix. This was also evidenced by the behavior of the nanocrystal melting points. This situation is confirmed with the TEM micrographs since the particles appear to be more defined with SDPH. Scattering curves (Figure 6) also display this effect since the SDPH nanoparticles have larger average size (correlation peak appears at smaller Q vector) than the NPP nanocrystals. These results suggest that hydrogen bonds between the dye and the host silicate matrix disturb the molecular aggregation. Moreover, increasing the dye concentration tends to increase the nanoparticles size.

When an external magnetic field is applied in situ during the nanocrystallization, the nanocrystal average sizes tend to increase. This is in agreement with the previously demonstrated[23] fact that the magnetic field reduces the disorder and aligns the NPP nanocrystals thanks to their large dipolar moment. Thus, the molecular aggregation becomes favored and leads to nanoparticles with larger average sizes, shifting the apex peak to lower Q values (Figure 7). This has been confirmed by calorimetry experiments which exhibit a slight decrease of the melting temperatures associated to a very narrow endothermal peak proving the good crystallinity of the nanocrystals.

Acknowledgment. The authors thank the analysis center of l'Institut de Recherches sur la Catalyze of Lyon for adsorption−desorption measurements and especially W. Desquesne. We are grateful to the Institut Laue Langevin neutron facility (ILL, Grenoble) for providing access to the neutron beam and all technical support during the experiments.

LA020878Z

(28) Mickelson, A. E.; Karklin, Ya Kh. *J. Cryst. Growth* **1981**, *52*, 524−529.

(29) Sanz, N.; Zaccaro, J.; Delmotte, L.; Le Luyer, C.; Ibanez, A. *J. Solid State Chem.* **2002**, *165*, 25−34.